Liquid-crystal periodic zigzags from geometrical and surface-anchoring-induced confinement: Origin and internal structure from mesoscopic scale to molecular level

Dong Ki Yoon,[1,2] Jinhwan Yoon,[3] Yun Ho Kim,[1] M. C. Choi,[4] Jehan Kim,[3] Osami Sakata,[5] Shigeru Kimura,[5] Mahn Won Kim,[6,7] Ivan I. Smalyukh,[2,8] Noel A. Clark,[2] Moonhor Ree,[3,*,†] and Hee-Tae Jung[1,*,‡]

[1]*Department of Chemical and Biomolecular Engineering (BK-21), Korea Advanced Institute of Science and Technology, Daejeon 305-701, Korea*

[2]*Department of Physics and Liquid Crystal Materials Research Center, University of Colorado, Boulder, Colorado 80309-0390, USA*

[3]*Department of Chemistry, Pohang Accelerator Laboratory, Center for Electro-Photo Behaviors in Advanced Molecular Systems, Division of Advanced Materials Science, Polymer Research Institute, and BK School of Molecular Science, Pohang University of Science & Technology, Pohang 790-784, Korea*

[4]*Department of Bio and Brain Engineering, Korea Advanced Institute of Science and Technology, Daejeon 305-701, Korea*

[5]*SPring-8/JASRI, Research & Utilization Division, Kouto 1-1-1, Sayo-cho, Sayo, Hyogo 679-5198, Japan*

[6]*Department of Physics, Korea Advanced Institute of Science and Technology, Daejeon 305-701, Korea*

[7]*Material Research Laboratory, University of California at Santa Barbara, Santa Barbara, California 93106, USA*

[8]*Renewable and Sustainable Energy Institute, UniversIty of Colorado at Boulder, Coulder, CO 30309, USA*

(Received 22 July 2010; published 15 October 2010)

We figured out periodic undulations of lamellae "zigzags" in liquid crystals under confinement by glass and patterned silicon hybrid cell, but in the absence of applied fields. The optical and internal structures of zigzags have been investigated from mesoscopic scale to molecular level by convoluting real and reciprocal space probes, such as polarized light microscopy, scanning electron microscopy, and microbeam x-ray diffraction. The homeotropic anchoring happens at air/liquid crystal, while planar one appears at glass or patterned silicon surfaces. The wetting and displacement of lamellae near the glass surface give rise to tilting and bending in the stacking of lamellae. This can provide a solution for the origin of periodic zigzags: asymmetric strain exerted to lamellae at two-dimensional glass surface and one-dimensional-like pattern. This can give a hint for potential photonic applications such as optical gratings and modulators due to its high periodicity.

DOI: 10.1103/PhysRevE.82.041705 PACS number(s): 61.30.Pq, 61.30.Cz, 61.30.Hn

I. INTRODUCTION

Currently there is great interest in understanding the self-organization of soft materials under conditions of nanoscale to microscale topographic confinement, and the key to exploiting such systems for advanced applications is the control of the structures adopted [1–7]. Often, it has been found that the combination of a three-dimensional confining geometry and the importance of the resulting inherent competition of surface interactions, especially important in small volumes, can lead to unexpected or undesirable organization. It is thus important to explore such self-organization in systems where detailed characterization and modeling of such confined structures can be obtained.

Fluid smectic layering, characterized by one-dimensional (1D) periodic ordering into liquidlike molecular layers, is one of the well-known structural themes in soft condensed materials, such as liquid crystals (LCs), block copolymers, supramolecules, and surfactants [1,4,6]. Inherent softness enables a variety of modes of control of the smectic layering system, making smectics particularly interesting for understanding the effects of nanoconfinement or microconfinement.

Here, we study a fluid smectic liquid crystal confined into micron-scale linear stripes by a combination of interfacial forces and topographic patterning (Fig. 1), revealing the roles of the layering elasticity, surface anchoring, and growth motif on the structures adopted. We find that the translational symmetry along the channel is spontaneously broken in the form of periodic zigzag smectic layer undulation patterns.

Because of the single dimension of periodic ordering, layer undulations are readily induced in such materials, for example, by applied electric and magnetic fields, dilative mechanical strain, and thermodynamic gradients [8–13]. In many cases undulations appear only above a critical value of external driving force, initially appearing as sinusoidal modulations, but then transforming to large deformation defects, such as focal conics for large driving forces [8,14,15]. The undulations appear in order to accommodate field-induced torque or strain in the presence of surface anchoring forces by enabling undulated layers in the medium with the constraint of flat layers near the boundaries. To understand the origin of these undulations, we probe the confined structure from the molecular to mesoscopic scales by real and reciprocal space probes including microbeam x-ray diffraction (mXRD), polarized optical microscopy (PLM), and electron microscopy techniques.

II. EXPERIMENT

Preparing confined lamellae of liquid crystals: Patterned silicon was fabricated on (100) Si wafers by using photolithography and reactive ion etching techniques. The patterns have square cross sections with certain depths, such as 2, 5,

*Corresponding author.
†ree@postech.edu
‡heetae@kaist.ac.kr

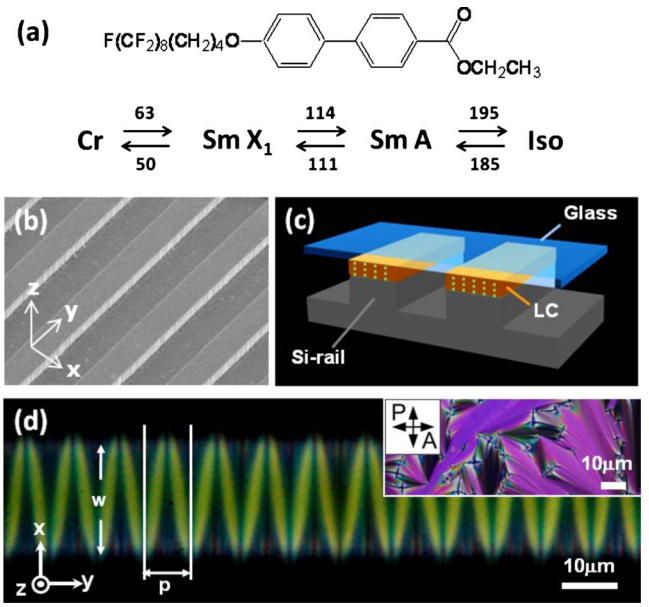

FIG. 1. (Color online) Sample preparation and optical zigzag pattern in the confined area. (a) The chemical structure and phases of liquid crystal 1 with transition temperatures in degrees centigrade. (b) SEM image of microchannels with 5 μm depth and 20 μm width. (c) The schematics represent the confined film of liquid crystal 1 (green dotted lines mean smectic layers) between on-top glass slide and microchannel in which 5 μm silica spacers were used. (d) PLM image of ordered zigzag morphologies of liquid crystal 1 in the confined condition with 20 μm channel; inset is the typical PLM image from the sandwiched slides. p is the pitch of optical zigzags, and w is the channel width.

and 10 μm, and vary in width from 3 to 100 μm. Regular silica microspheres (2–10 μm) were used for controlling space between glass and patterned silicon. To control the surface anchoring, the glass and patterned surfaces were chemically cleaned by immersion in a mixture of dimethylformamide and methanol to remove organic-inorganic impurity, followed by rinsing several times with de-ionized water. Then, two surfaces, patterned silicon and glass, were spin coated with a fluorinated polymer (Teflon-AF®, Dupont) in organic fluorinated solvent (FluorinertTM FC-77, 3 M) to obtain planar anchoring of this semifluorinated LC (Sm*A* layers normal to the surface). During the sample loading, the glass-patterned silicon hybrid cell equipped with a hot stage (Mettler FP82 HT) was heated to a temperature above the smectic-isotropic transition temperature (194.7 °C) to facilitate the flow of material 1 into the cell, and cooled down at −2 °C/min.

mXRD: The mXRD measurements were carried out at the BL13XU of the SPring-8 (Fig. S5 in the supplementary material [17]). A focused x-ray beam of 1 μm size with energy of 11 keV was used. Samples were mounted on a homemade helium chamber equipped with 100 nm resolved *xyz* high-precision linear motor stages. The sample-to-detector distance was 165 mm, and data were collected for 60 s with a two-dimensional (2D) charge-coupled device detector (Roper Scientific, Trenton, NJ).

Polarized optical and electron microscopy: The optical anisotropic textures were observed under polarized optical microscopy Leica DMLB. For scanning electron microscopy (SEMs), confined LC films were fractured in the liquid nitrogen, coated with a 5 nm layer of Pt, and imaged using FEI Serion FE-SEM at National Nanofab Center (NNFC) in Korea Advanced Institute of Science and Technology (KAIST).

III. RESULTS

The rod-shaped liquid crystal 1, 4′-(5,5,6,6,7,7,8,8,9,9,10,10,11,11,12,12,12-heptadecafluorododecyloxy)-biphenyl-4-carboxylic acid ethyl ester, was synthesized according to the method previously reported [Fig. 1(a) and Figs. S1 and S2 in the supplementary material] [4,16,17]. The thermal phase transition of liquid crystal 1 exhibits a transition upon cooling from the isotropic to a smectic-*A* phase $T=185$ °C, and then from the smectic *A* to a soft crystal (Sm*X*) phase at $T=111$ °C. The smectic LC structure of liquid crystal 1 was studied by XRD on 1-mm-diameter and 1-mm-thick bulk sample that was sealed by polyimide film in copper cell, which exhibited large domains of single layer orientation. mXRD was also carried out on oriented regions in the channel cell described below.

The single domain mXRD patterns in Fig. 3(b) show several sharp peaks in the small angle between $q=1.0$ nm^{-1} and $q=6.0$ nm^{-1}. The q-space structure is very similar to the case of bilayered fluid smectic phase in polar compounds which have a strong tendency for local polar bilayer ordering [18,19]. The polar semifluorinated tails of liquid crystal 1 cause splayed molecular stacking in Fig. 3(c), which depends on dipole delocalization [19]. Based on this configuration, some peaks are located on the meridional line, *n*, but mostly are split from the meridional line, indicative of a modulated layer structure. The peak positions accurately match with the body-centered rectangular structure in unit cell of $a=6.02$ nm and $c=7.20$ nm. Additionally, three diffuse peaks observed in the wide angle, $R1=12.6$ nm^{-1}, $R2=15.3$ nm^{-1}, and $R3=17.0$ nm^{-1}, indicate distributions of orientation in the tail and aromatic groups. The molecular level structure of the Sm*A* phase of liquid crystal 1 was established from these data and the molecular simulation software package CERIUS2 (Accelrys, San Diego, CA, USA). As in Fig. 3(c), liquid crystal 1 is stabilized with attractive π stacking interaction between adjacent biphenyl groups, and the d spacing of liquid crystal 1 is ~3.52 nm. From the $R1$ peak the mean distance between the semifluoroalkyl chains of ~0.50 nm and $R2$ is related to the width of the biphenyl cores, ~0.41 nm. $R3$ indicates the typical face-to-face distance between flat aromatic molecules (biphenyl group), ~0.37 nm. This body-centered rectangular structure is typical for modulated smectic-*A* phases [20].

In the confinement experiments a thin film of liquid crystal 1 was contained in a hybrid cell made from a glass plate and a topographically patterned silicon wafer [Fig. 1(b)]. The topographic pattern on the silicon has channels of length of 10 mm; depths of 2, 5, and 10 μm; and widths w in the range $3<w<100$ μm. Silica microspheres of diameter d, with $2<d<10$ μm, were used to determine the glass/silicon spacing to achieve LC films of constant thickness d.

The two surfaces, patterned silicon and glass, were spin coated with a fluorinated polymer (Teflon-AF®, Dupont) in organic fluorinated solvent (FluorinertTM FC-77, 3 M) to obtain planar anchoring of this semifluorinated LC (Sm*A* layers normal to the surface). During the loading, the sample was heated to a temperature above the smectic-isotropic transition temperature to facilitate the capillary flow of the LC only into the space between the top of the patterned silicon rails and the glass [Fig. 1(c)], followed by cooling to room temperature. The resulting linear strips of LC are bounded by glass on the top, silicon on the bottom, and air on the two sides. The surface anchoring of LC is planar (Sm*A* layers normal to the surface) at the silicon and glass interfaces, and homeotropic (layers parallel to the surface) at the air/LC interface [4,21]. This combination of orientations is consistent with the simple "bookshelf" alignment of the Sm*A* layers, shown in Fig. 1(c) (green lines in orange LC region).

Figure 1(d) shows however that the layer organization is more complex, exhibiting optical zigzag patterns when viewed between crossed polarizers. These patterns are quite uniform in structure in patches and reach the entire 10 mm length of the cell. The pitch p of the zigzags is defined in Fig. 1(d). Given the boundary conditions it appears that in the dark areas of Fig. 1(d) the LC director $\mathbf{n}(\mathbf{r})$, giving the local mean molecular long axis, is parallel to the polarizer axis (x), whereas in the bright regions $\mathbf{n}(\mathbf{r})$ is rotated relative to the polarizer axis, i.e., the zigzags are indicative of the modulation of the orientation of $\mathbf{n}(\mathbf{r})$ in alternating fashion along the confined LC stripes. In a Sm*A* phase, since $\mathbf{n}(\mathbf{r})$ is locally along the layer normal, such periodic reorientation of $\mathbf{n}(\mathbf{r})$ must be accompanied by a zigzag pattern of layer undulation. The optical zigzags increase in pitch as the width and depth of the LC stripe are increased (Figs. S3 and S4 in the supplementary material [17]). In the example of Fig. 1(d), where $w=20$ μm and $d=3$ μm, the pitch of the zigzags is $p\sim 8$ μm [Fig. 1(d)]. In glass/glass cells ($d=5$ μm) with similar surface treatment planar alignment is achieved, but optical zigzags have not been observed [inset of Fig. 1(d)], implying that zigzags are the result of the confined geometry.

The formation process of the optical zigzags can be followed during cooling from the isotropic phase by PLM, and it is found that the first appearance of the Sm*A* phase is as triangular Sm*A* domains nucleating on the air/LC interfaces of the LC stripe sides, and growing toward the center of the LC stripe (Fig. 2). As is typically the case, the Sm*A* layers are normal to the growing isotropic/Sm*A* interface. As a result the Sm*A* grows in the form of a series of bâtonnetlike domains [22]. These growth structures, schemed in the yellow box in Fig. 2(a), leave behind a pattern of undulated Sm*A* layers, evidenced by the short pitch periodic pattern of molecular tilt within the triangles. When the growth fronts traverse the width of the stripes the growing isotropic/Sm*A* interface disappears, and there is a distinct transition from the fine texture of the growth triangles to the zigzag structures with longer pitch [Fig. 2(b)]. The appearance for a final zigzag layer structure is a direct consequence of the short pitch undulations in the growth triangles. If we consider the contour length $|\mathbf{L}|=\int(\mathbf{z}\times\mathbf{n})dy$ of the layers in the growth triangles, we must have $|\mathbf{L}|>\int dy$, and once the Sm*A* layering is established this condition must be maintained, requiring undulated layers. Energy minimization will lead to a longer pitch of the final structure, with the initial short pitch being a consequence of the growth kinetics. This is a form of the mechanically induced undulation instability [10,11], where instead of being produced by dilative stress normal to the layers, it is produced by excess layer area and a resulting compressive stress parallel to the layers.

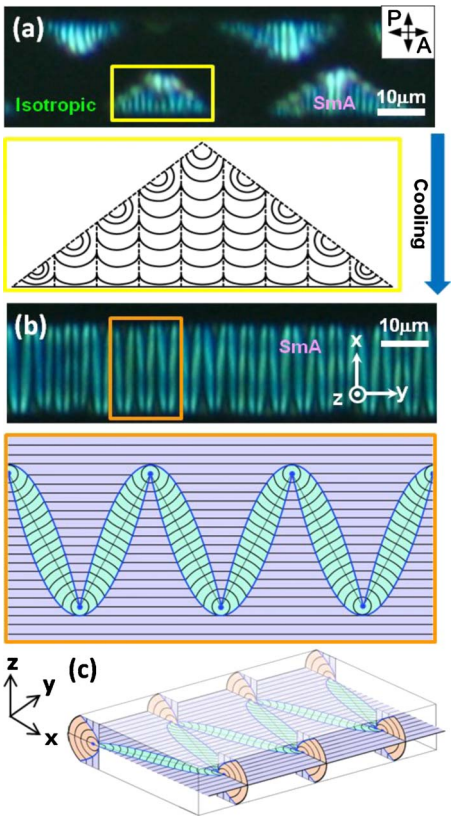

FIG. 2. (Color online) The PLM image and scheme for forming process of optical zigzags in the confined geometries. (a) Initial state of the optical triangular growth of smectic region looks like bâtonnet structure containing focal conic domain, and the corresponding scheme shows how to grow the triangular textures from each side area of patterned silicon rail of air boundary. (b) After collapse of each domain, periodic optical zigzags are clearly shown in PLM image, and this is caused by parabolic wall arrangement of smectic layers based on the initial focal conic domains as shown in the scheme. (c) Three-dimensional scheme of parabola domains in smectic film.

To elucidate the molecular level structure of the confined zigzags, mXRD experiments were carried out in three specific positions along y of the zigzag formed on $w=20$ μm LC stripes [Fig. 3(a)]. Since the beam size of x ray $\sim 1\times 1$ μm^2 is smaller than p, the internal zigzag structure can be probed [23,24]. The details in mXRD setup are described in Fig. S5 in the supplementary material [17]. Figure 3(a) shows three distinct mXRD patterns D1, D2, and D3 measured from three specific positions in zigzag, A1, A2, and A3, respectively. The features of diffraction pattern are following: A lattice of sharp spots is seen at small angle with the 00l direction indicting the Sm*A* layer normal n and azimuthally diffuse wide angle peaks are seen at large angle in the direction of the layer planes. These features match the

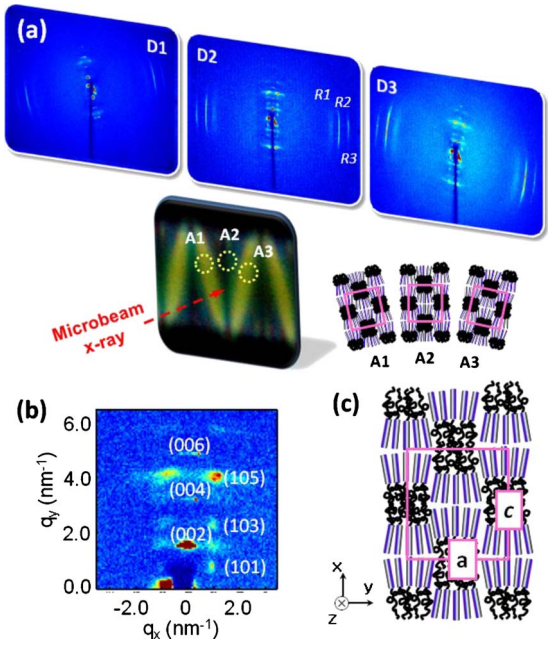

FIG. 3. (Color online) mXRD patterns of zigzag patterns through the microchannel. (a) X-ray diffraction patterns of D1, D2, and D3 from scanning of single zigzag morphology of A1, A2, and A3, respectively. (b), The enlarged mXRD pattern of D2. (c) The rectangular structure of liquid crystal 1 with a=6.02 nm and c=7.21 nm, revealed by mXRD and molecular simulation, revealing that this is modulated Sm*A* phase.

bulk XRD pattern. The XRD patterns obtained at A1–A3 exhibit the same structure, differing only in their overall orientation. At A2, which is in the dark region of the zigzag, the 00l small angle peaks are lined up along x, i.e., normal to the stripe direction. At A1 (A3) they are rotated 9° counterclockwise (clockwise) relative to that of A2, confirming that layer undulation accompanies the optical zigzags. Figure 3(c) indicates the Sm*A* modulation orientation producing the scattering in Fig. 3(a), i.e., with the **a**-**c** plane parallel to the glass. The confined sample may be a single domain of this modulation orientation, or the modulation lattice may be orientationally disordered about n.

The mechanism leading to undulation formation proposed above leads, near threshold, to smoothly undulated layers. However, the zigzag structure as grown in the cells exhibits a distinct alternation between layer segments running parallel to the channel (normal in the x-z plane), which show up dark in Figs. 1(b) and 2(c), and Figs. S3 and S4(b) of the supplementary material [17], and segments rotated about z, which show up bright in these images, suggestive of an internal structure that is more complex than simple undulations. More systematic experiments and their relationship will be discussed in near future. Study of the evolution of undulation textures in smectics and chiral nematics shows that smooth undulations are confined to a rather narrow range of dilations and with increasing dilation give way to focal conic defects, in particular periodic arrays of parabolic focal conics (PFCs), or nested PFCs [8,10,14,15]. These defect arrays introduce a core of multiply connected curved layers that have nearly the zero-stress layer spacing everywhere, thereby reducing the elastic energy associated with accommodation of a square lattice of layer undulations. We find that the nested PFC model, initially developed to describe the undulation pattern in chiral nematics at large dilation, provides an excellent description of the liquid crystal 1 Sm*A* undulation pattern in the Sm*A* sample, making this an observation of the nested PFC structure in smectics [8]. The nested PFC structures are sketched in Figs. 2(b) and 2(c), showing the confocal parabolic defects in orthogonal planes, with a periodic sheet of nested parabola along the channel in the x-y plane. These parabolas mediate distinct transitions in layer orientation of just the type required to account for the PLM images in Figs. 1(b) and 2(c), and Figs. S3 and S4(b) of the supplementary material [17].

We also investigated the internal structure of zigzags, using scanning electron microscopy (SEM) on cells with w=10 μm. In these experiments the LC stripe cells in the Sm*A* temperature range were quenched in liquid N_2, the glass slide was removed, the cell was sectioned, and the section was visualized by SEM. Figure 4 shows that the lamellae layers are on average normal to the substrates, but exhibit distinctive patterns of local layer tilt in the x-z plane and of undulations along y. This layer tilt changes discontinuously through angles as large as 50° and is reminiscent of the layer bends in the chevron structure observed in smectic samples grown in thin gaps between flat plates and then subjected to layer shrinkage, for example, at a Sm*A* to Sm*C* phase transition [25]. Especially, cross-sectioned layers have double-kinked shape that are bent (θ_b) and tilted (θ_t) [Fig. 4(a)] to satisfy the boundary condition of air and silicon-glass hybrid cell, in which θ_b is the bending angle between kinked smectic layers, and θ_t is the tilt angle between smectic layers and silicon substrate. Basically, normal chevron structure is formed during transition from Sm*A* to Sm*C* phase, and this compression makes smectic layers kink in the middle of film. However, here the hybrid boundary condition of silicon, glass, and air makes our system be transformed based on normal chevron structure. This distortion has been observed not only near LC/air interface [black arrow, Fig. 4(b)], but also at the center of the film [white arrow, Fig. 4(b)]. Also evident in Figs. 4(b) and 4(e) is the undulation along the channel direction, with the top front view in Fig. 4(e) (black star) and top-side views in Fig. 4(c) (white star) clearly showing their undulating features. Additionally, in Fig. 4(e), the bend direction is alternating from the left (dotted line in green) to right (solid line in yellow) for sections at different y positions, a direct consequence of the layer undulation. The cross-sectioned images suggest smectic-*C*-style zigzag defects as a motif for the zigzag layer undulation, as sketched in Figs. 4(g) and 4(h), where the reoriented diamond-shaped layer segments at the zigzag wall show up as the bright areas in the PLM images [26,27]. Since the zigzag walls run at an oblique angle across the stripe, sections in the x-z plane start in one side of a wall and end up on the other side of the wall, leading to gradual progression of the bends from one end in x to the other [Figs. 4(g) and 4(h)]. The whole stripe cross-section area (see Fig. S6 in the supplementary material for additional SEM results [17]) suggests that the contact angle at the LC/glass/air contact line is ~45°, increasing the width of the stripe as the glass is approached.

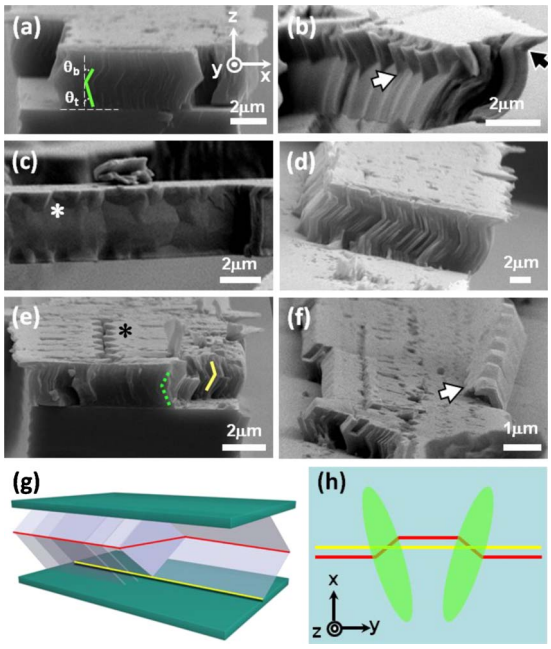

FIG. 4. (Color online) Scanning electron micrograph images of cross-sectioned sample of confined liquid crystals film between microchannel with 10 μm width and on-top glass slide; its scheme. (a) Top front view of layer distortions; bent by $\theta_b \sim 50°$ and tilted by $\theta_t \sim 67°$. (b) The layer distortions in lamellae appear not only at LC/air interface (black arrow), but also near the center of the film (white arrow). (c) Top side views: ripplelike ridges are alternating through the channel. (d) Double-kinked smectic layers in the intermediate region between dimple structure that can be seen in PLM image and scheme. (e) The top front view of the sample. The direction of the bent layers is alternating from the left in the front (green dotted line) to the right (yellow solid line) as it moved along the microchannel. (f) Fractured intermediate sidewall shows how smectic layers are bent (arrow), which is developed from the outer sidewall in the air. (g) Scheme of internal structure of smectic layers in the zigzag pattern; the direction of periodic vertical smectic layers is changed via diamond plane. Red/dark gray and yellow/light gray lines mean contour lines through the kinked center and bottom line of smectic layers, respectively. (h) Top view of (g) shows how contour lines go through the channels. Green ellipsoidal area means bright optical domains in PLM images.

The contour line [parabolic wall (PW)] in the schematics in Figs. 2(c), 4(g), and 4(h) can be preserved because the energy density of focal conic domains is not strong to overcome the movement of molecules from one to another layers to be flat smectic layers eventually. To estimate the energy of the zigzag patterns, one can follow a similar procedure to that reported in Ref. [8], calculating the total free energy. The main feature of the packing of layers in PW structures is that the strongly tilted layers at the boundary area coexist with the flat layers. According to previous elastic energy calculation for PWs [8], a straightforward calculation yields $F_{wall}^{PW} \approx KL/\lambda$. K is a curvature modulus, L is a length of one pair zigzag pattern, λ is the smectic penetration length ($\lambda = \sqrt{K/B}$), and B is a compression modulus that describes the elastic resistance to changes (δ) in the smectic layer thickness. Thus, the formation of optical zigzag pattern in a channel results from the balance of surface anchoring energy (F_W) and elastic energy (F_{wall}^{PW}) induced in the PWs. The anchoring energy density for large tilts is on the order of $W_{\chi 0}$. For the typical experimental values [28] $W_{\chi 0} \sim (0.1-1) \times 10^{-4}$ J/m^2, it is comparable or larger than the elastic energy density carried by the PWs (or the walls in zigzag pattern) [29], $\sim 4F_{wall}^{PW}/L \sim 4K/\lambda \sim 0.4 \times 10^{-4}$ J/m. It means that optical zigzag pattern was produced by strong surface anchoring at the boundary surface such as air-contacted area in a confined sandwich channel cell.

IV. CONCLUSION

In summary, we discovered that periodic undulations of lamellae zigzags in liquid crystals are generated under confinement by glass-patterned silicon hybrid cell, but in the absence of applied fields. By convoluting real and reciprocal space probes, such as polarized light and scanning electron microscopy and mXRD, the internal structures of zigzags have been investigated from mesoscopic scale to molecular level: the body-centered rectangular structure with the c axis where molecule 1 lies being normal to the patterned silicon, the homeotropic anchoring at air/LC and planar at glass or patterned silicon surfaces, the wetting and displacement of lamellae near the glass surface giving rise to tilt, and bent in the stacking of lamellae. This gave a hint for the origin of periodic zigzags: asymmetric strain exerted to lamellae at 2D glass surface and 1D-like pattern; the latter is strain-free. Further, this opens up the possibility on photonic applications such as optical gratings and modulators due to its regular shape.

ACKNOWLEDGMENTS

We thank Professors O. D. Lavrentovich and T. C. Lubensky for insightful discussions. This work was supported by the National Research Laboratory (NRL) Program No. R0A-2007-000-20037-0; World Class University (WCU) Programs No. R32-2008-000-10142-0, No. R33-2008-000-10163-0, and No. R31-2008-000-10059-0; Basic Science Research Program (Grant No. 2009-0087691); and Grants No. NRF-2009-352-D00088 and No. 2010-000-1784 (SRC) through the National Research Foundation of Korea funded by the Ministry of Education, Science and Technology (MEST) and the Korea Healthcare Technology R&D Project by Ministry for Health, Welfare & Family Affairs A040041. This work was also supported by MRSEC Program by NSF Grant No. DMR-0820579, and I2CAM Junior Exchange Award by NSF Grant No. DMR-0645461 under ICAM-I2CAM. Synchrotron x-ray diffraction measurements were supported in part by MEST, POSCO, and POSTECH Foundation; microbeam x-ray diffraction experiments were performed at SPring-8 BL13XU (Contract No. 2006B1768); and FE-SEM experiments were executed at NNFC in KAIST.

[1] J. Y. Cheng, C. A. Ross, H. I. Smith, and E. L. Thomas, Adv. Mater. **18**, 2505 (2006).
[2] I. Bita, J. K. W. Yang, Y. S. Jung, C. A. Ross, E. L. Thomas, and K. K. Berggren, Science **321**, 939 (2008).
[3] E. Vekris, V. Kitaev, D. D. Perovic, J. S. Aitchison, and G. A. Ozin, Adv. Mater. **20**, 1110 (2008).
[4] D. K. Yoon, M. C. Choi, Y. H. Kim, M. W. Kim, O. D. Lavrentovich, and H.-T. Jung, Nature Mater. **6**, 866 (2007).
[5] R. A. Segalman, H. Yokoyama, and E. J. Kramer, Adv. Mater. **13**, 1152 (2001).
[6] S. O. Kim, H. H. Solak, M. P. Stoykovich, N. J. Ferrier, J. J. de Pablo, and P. F. Nealey, Nature (London) **424**, 411 (2003).
[7] Y. N. Xia, Y. D. Yin, Y. Lu, and J. McLellan, Adv. Funct. Mater. **13**, 907 (2003).
[8] B. I. Senyuk, I. I. Smalyukh, and O. D. Lavrentovich, Phys. Rev. E **74**, 011712 (2006).
[9] T. Ishikawa and O. D. Lavrentovich, Phys. Rev. E **63**, 030501(R) (2001).
[10] N. A. Clark and R. B. Meyer, Appl. Phys. Lett. **22**, 493 (1973).
[11] N. A. Clark and P. S. Pershan, Phys. Rev. Lett. **30**, 3 (1973).
[12] M. Delaye, R. Ribotta, and G. Durand, Phys. Lett. A **44**, 139 (1973).
[13] M. Reznikov, B. Wall, M. A. Handschy, and P. J. Bos, J. Appl. Phys. **104**, 044902 (2008).
[14] C. S. Rosenblatt, R. Pindak, N. A. Clark, and R. B. Meyer, J. Phys. (Paris) **38**, 1105 (1977).
[15] N. A. Clark and A. J. Hurd, J. Phys. (Paris) **43**, 1159 (1982).
[16] V. Percec, G. Johansson, G. Ungar, and J. P. Zhou, J. Am. Chem. Soc. **118**, 9855 (1996).
[17] See supplementary material at http://link.aps.org/supplemental/10.1103/PhysRevE.82.041705. This includes material, experimental set-up, optical and electron microscopy images.
[18] F. Hardouin, M. F. Achard, C. Destrade, and N. H. Tinh, J. Phys. (Paris) **45**, 765 (1984).
[19] F. Hardouin, Physica A **140**, 359 (1986).
[20] J. Prost and P. Barois, J. Chim. Phys. Phys.-Chim. Biol. **80**, 65 (1983).
[21] M. C. Choi, T. Pfohl, Z. Y. Wen, Y. L. Li, M. W. Kim, J. N. Israelachvili, and C. R. Safinya, Proc. Natl. Acad. Sci. U.S.A. **101**, 17340 (2004).
[22] J. B. Fournier and G. Durand, J. Phys. II **1**, 845 (1991).
[23] S. Kimura, Y. Kagoshima, K. Kobayashi, K. Izumi, Y. Sakata, S. Sudo, Y. Yokoyama, T. Niimi, Y. Tsusaka, and J. Matsui, Jpn. J. Appl. Phys., Part 2 **41**, L1013 (2002).
[24] A. Iida, Y. Takahashi, Y. Takanishi, M. Nakata, K. Ishikawa, and H. Takezoe, Liq. Cryst. **32**, 717 (2005).
[25] S. Martellucci and A. N. Chester, *Phase Transitions in Liquid Crystals* (Plenum Press, New York, 1992).
[26] N. A. Clark and T. P. Rieker, Phys. Rev. A **37**, 1053(R) (1988).
[27] N. A. Clark, T. P. Rieker, and J. E. Maclennan, Ferroelectrics **85**, 467 (1988).
[28] I. I. Smalyukh and O. D. Lavrentovich, Phys. Rev. Lett. **90**, 085503 (2003).
[29] O. D. Lavrentovich, M. Kleman, and V. M. Pergamenshchik, J. Phys. II **4**, 377 (1994).